Intracellular host cell membrane remodelling induced by SARS-CoV-2 infection *in vitro*

Lucio Ayres Caldas*†[1,2] (ID) **, Fabiana Avila Carneiro*** (ID) **, Fabio Luis Monteiro‡** (ID) **, Ingrid Augusto†** (ID) **,
Luiza Mendonça Higa‡** (ID) **, Kildare Miranda†§** (ID) **, Amilcar Tanuri‡** (ID) **and Wanderley de Souza†§** (ID)

*Núcleo Multidisciplinar de Pesquisas em Biologia - NUMPEX-BIO, Campus Duque de Caxias Geraldo Cidade, Universidade Federal do Rio de Janeiro, Rio de Janeiro, Duque de Caxias, RJ, Brazil, †Laboratório de Ultraestrutura Celular Hertha Meyer, Instituto de Biofísica Carlos Chagas Filho, Universidade Federal do Rio de Janeiro, Brazil, ‡Departamento de Genética, Instituto de Biologia, Universidade Federal do Rio de Janeiro, Rio de Janeiro, Brazil, and §Instituto Nacional de Ciência e Tecnologia de Biologia Estrutural e Bioimagem (INBEB) and Centro Nacional de Biologia Estutural e Bioimagen (CENABIO), Universidade Federal do Rio de Janeiro, Rio de Janeiro, Brazil

Background Information. Severe acute respiratory syndrome coronavirus-2 (SARS-CoV-2) infection induces an alteration in the endomembrane system of the mammalian cells. In this study, we used transmission electron microscopy and electron tomography to investigate the main structural alterations in the cytoplasm of Vero cells infected with a SARS-CoV-2 isolate from São Paulo state (Brazil).

Results. Different membranous structures derived from the zippered endoplasmic reticulum were observed along with virus assembly through membrane budding. Also, we demonstrated the occurrence of annulate lamellae in the cytoplasm of infected cells and the presence of virus particles in the perinuclear space.

Conclusions and Significance. This study contributes to a better understanding of the cell biology of SARS-CoV-2 and the mechanisms of the interaction of the virus with the host cell that promote morphological changes, recruitment of organelles and cell components, in a context of a virus-induced membrane remodelling.

Additional supporting information may be found online in the Supporting Information section at the end of the article.

Intracellular membranes in SARS-CoV-2 morphogenesis

The severe acute respiratory syndrome coronavirus-2 (SARS-CoV-2) was the third human coronavirus responsible for severe respiratory diseases in the last two decades, preceded by severe acute respiratory syndrome (SARS) and Middle East respiratory syndrome (MERS) viruses (Zhong et al., 2003; Zaki et al., 2012; Zhu et al., 2020). As coronaviruses are known to infect animals, primarily, humans' infection results from virus spillover (Rabaan et al., 2020).

The ongoing SARS-CoV-2 pandemic resulted in worldwide quarantine implementation and physical distancing (WHO, 2020), but the lack of knowledge of the coronavirus disease-2019 (COVID-19) physio and cytopathology is currently one of the barriers to disease control. Understanding the biology of SARS-CoV-2 interaction with the cell is fundamental to elaborating new intervention strategies.

Belonging to the *Coronaviridae* family and Betacoronavirus genus, SARS-CoV-2 presents a positive-stranded RNA genome encased by the nucleocapsid protein (N) and surrounded by the membrane protein

(M) and an envelope protein (E). The spike protein (S) projected from the viral envelope is crucial for virus internalisation and antigenicity (Lu et al., 2020; Walls et al., 2020). After attachment and internalisation, the viral genome is released in the cytoplasm and translated into two polyproteins and structural proteins. Simultaneously, the complex replication step involves synthesising subgenomic RNAs and accessory proteins before assembly and maturation in the endoplasmic reticulum-Golgi intermediate compartment (ERGIC) and Golgi apparatus (Alsaadi & Jones, 2019; Sicari et al., 2020).

Similar to other positive-sense RNA viruses, coronavirus infection induces an intense membrane remodelling in the cell cytoplasm. Virus replication is benefited by these membrane remodelling that protects the synthesis of viral RNA and the formation of replication–transcription complexes (Miller and Krijnse-Locker, 2008). It is well established that different viruses have their membrane complexes derived from specific cellular organelles, for example, the external mitochondrial membrane, the ER (Gillespie et al., 2010), the Golgi apparatus (Hansen et al., 2017) or the plasma membrane (Spuul et al., 2010). This large area dedicated to the virus replication and morphogenesis is known by different designations, such as viral factory or viroplasm, for example (Netherton and Wileman, 2011).

Among the different types of membrane arrangements (probably derived from the endoplasmic reticulum (ER)) described in the cytosol of coronavirus-infected cells, the spherules, the convoluted membrane (CM), the vesicle packet, and the so-called double-membrane vesicles (DMVs), that appear to have a crucial role in virus replication and morphogenesis (Knoops et al., 2008).

In a previous study, we approached by high-resolution scanning electron microscopy (SEM), the morphological alterations on Vero cells infected by SARS-CoV-2 isolated from São Paulo State of Brazil (SARS-CoV-2 SP). Also, we explored some features of cell-to-cell virus propagation (Caldas et al., 2020a). In this work, we studied the interaction of this isolate with Vero cells by transmission electron microscopy (TEM). We aimed to identify, using electron tomography followed by three-dimensional reconstruction, the compartments involved in the replication and morphogenesis steps of infection.

Results

Coronavirus-infected cells display a robust array of membranes that configures a platform for virus replication, assembly and maturation. We explored the main features of the infection of Vero cells with SARS-CoV-2 SP at 24 and 48 hours post-infection (hpi), giving special attention to the cytoplasmic alterations induced during the virus replication and morphogenesis. Due to these arrangements' complexity, the visualisation of these features required TEM and electron tomography.

The panoramic indications of such cytosolic disturbances triggered by SARS-CoV-2 SP were evident at 24 hpi (Figures 1A and 1B), where CMs were present in the perinuclear area and DMVs were abundant through the cytoplasm. Forming vesicle packets (>1 μm in size), spherules and budding of virus-like particles were also observed in this time of infection (Figure 1C). We identified regions of zippered ER next to DMVs in the cytoplasm of 48 hpi cells (Figure 1D) and interposed between clusters of DMVs and peripheral virus-containing compartments (Figure 1E). Tubular membrane connections containing virus-like particles were observed to contact the mitochondrial outer membrane (Figure 1F). The interior of DMVs was filled with filamentous material.

Once the zippered ER has nucleated the membrane rearrangements mainly constituted by spherules and DMVs (Figure 2A), nascent viruses are processed. They can be found at Golgi cisternae in the maturation step (Figures 2B and 2C). The clusters of intramembranous arrangements displayed large virion-containing vacuoles (LVCV) localised in the viral factory's frontier (Figure 2D). Further inspection of these areas revealed the accumulation of an electron-dense material within the inner face of a DMV (Figure 2E) and virus budding sites located on smooth vacuoles (Figures 2F–2H).

In the last step before the virus release into these vacuoles, a membrane belt can be distinguished as a bond between the virus and the smooth vacuole (Figure 3A). Once disconnected from the smooth vacuole membrane, the viruses remain adhered to their inner layer (Figure 3B). Intriguingly, long membrane excerpts seem to wrap more than one viral particle (Figure 3C). Figure 3D shows three different virus interaction moments with smooth vesicles: virus budding, adhesion and free virus in the vesicle lumen.

Figure 1 | Transmission electron microscopy of the membrane rearrangements induced by SARS-CoV-2 infection at 24 and 48 hpi (A) Panoramic view of a mock-infected Vero cell showing pattern distribution of organelles. **(B)** At 24 hpi, convoluted membranes (cm) and double-membrane vesicles (*) distribution in the infected cell could be seen. **(C)** Perinuclear area of the viroplasm showing DMVs invaginations (asterisk), virus-containing smooth vacuole (arrow) and virion release (arrowhead). **(D)** At 48 hpi, zippered ER (zr) was observed in continuity with DMVs (arrow). **(E)** Zippered ER (zr) was observed in the border between clusters of DMVs containing filamentous material (asterisk) and the areas where large vacuoles containing virus (arrows) are abundant. Arrowhead filled in white indicates a viral budding at the DMVs area. Black arrowheads indicate virus particles inside a large smooth vacuole, and viruses adhered to the cell surface. In **(F)**, apposed to the mitochondria, a tubular membrane containing virus-like particles (arrows), also flanked by DMVs (*). er, endoplasmic reticulum; g, Golgi apparatus; m, mitochondria; n, nucleus.
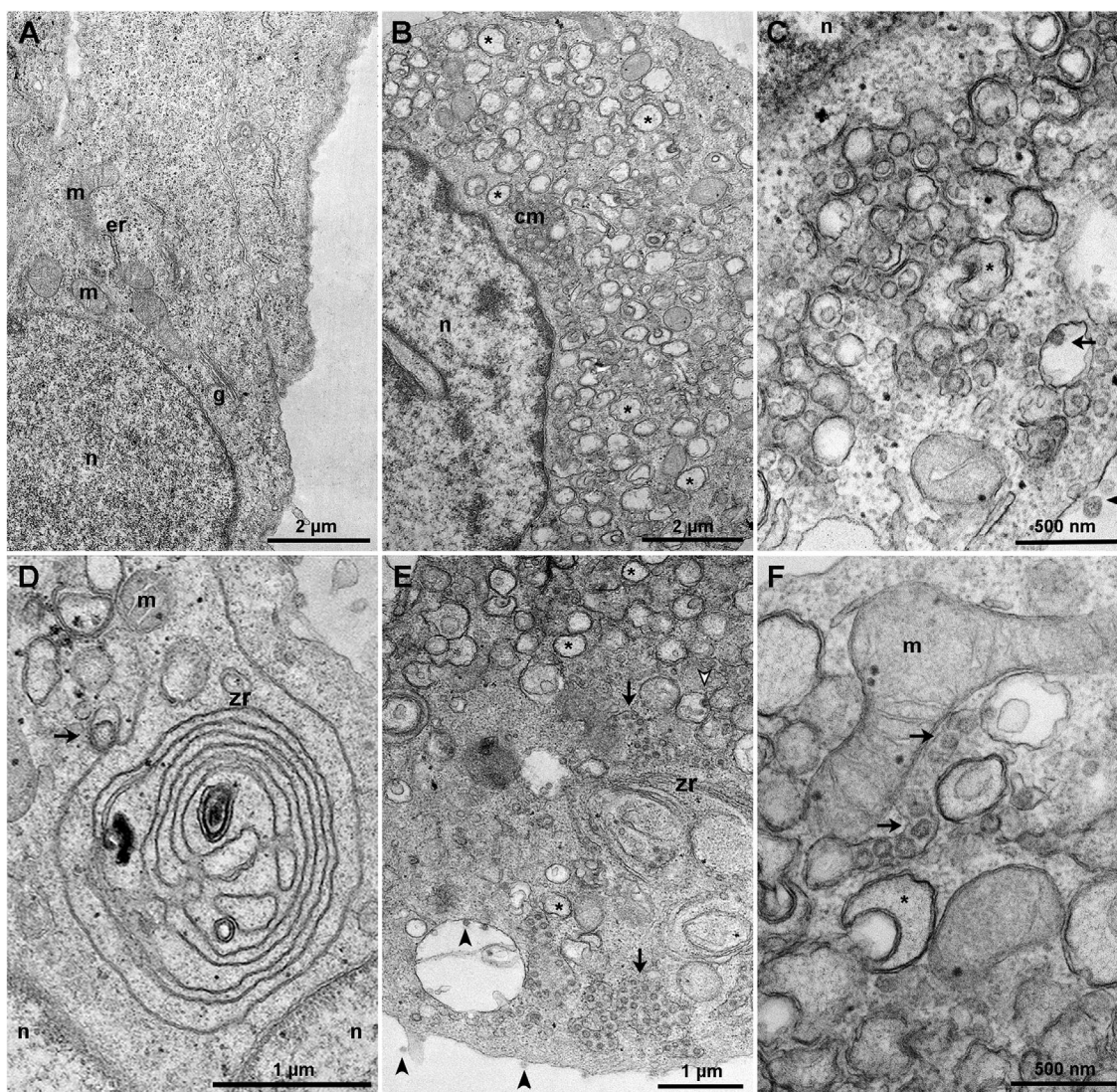
The observation of transversally sectioned tubular compartments revealed the presence of LVCV, suggesting that this compartment grows from the intermembrane space of DMVs (Figure 3E). Intriguingly, at 48 hpi, parallel arrays of cisternae-like structures containing interspaced circular shapes were displayed in approximately 10% of the observed sections of infected cells (Figure 3F). Among 109 cells

Figure 2 | Transmission electron microscopy of the distinct patterns of membrane arrangements during SARS-CoV-2 processing (**A**) Membrane complex formed from the zipped ER (arrow), with DMVs (asterisk) and spherules (arrowhead). (**B**) Nascent viruses (arrow) are processed in the Golgi apparatus (g) next to mitochondria (m) and a LVCV (arrowhead). (**C**) Higher magnification of a Golgi apparatus and recently processed viruses (arrows). (**D**) A delimited viroplasmic area displaying clusters of tubular structures containing spherules (arrow) is followed by the presence of LVCVs (arrowhead) at the periphery of the cytosol. The long arrows indicate viruses adhered to the cell surface. (**E**) Accumulation of electron-dense material was indicated by arrows in DMV and (**F**) the locus of virus assembly through budding into membrane clusters. Arrowhead points to a viral particle adhered to the inner face of the smooth vacuole. The budding event was further explored in (**G**) and (**H**), in which the membrane arrangements wrap the electron-dense material during virus assembly (arrow).
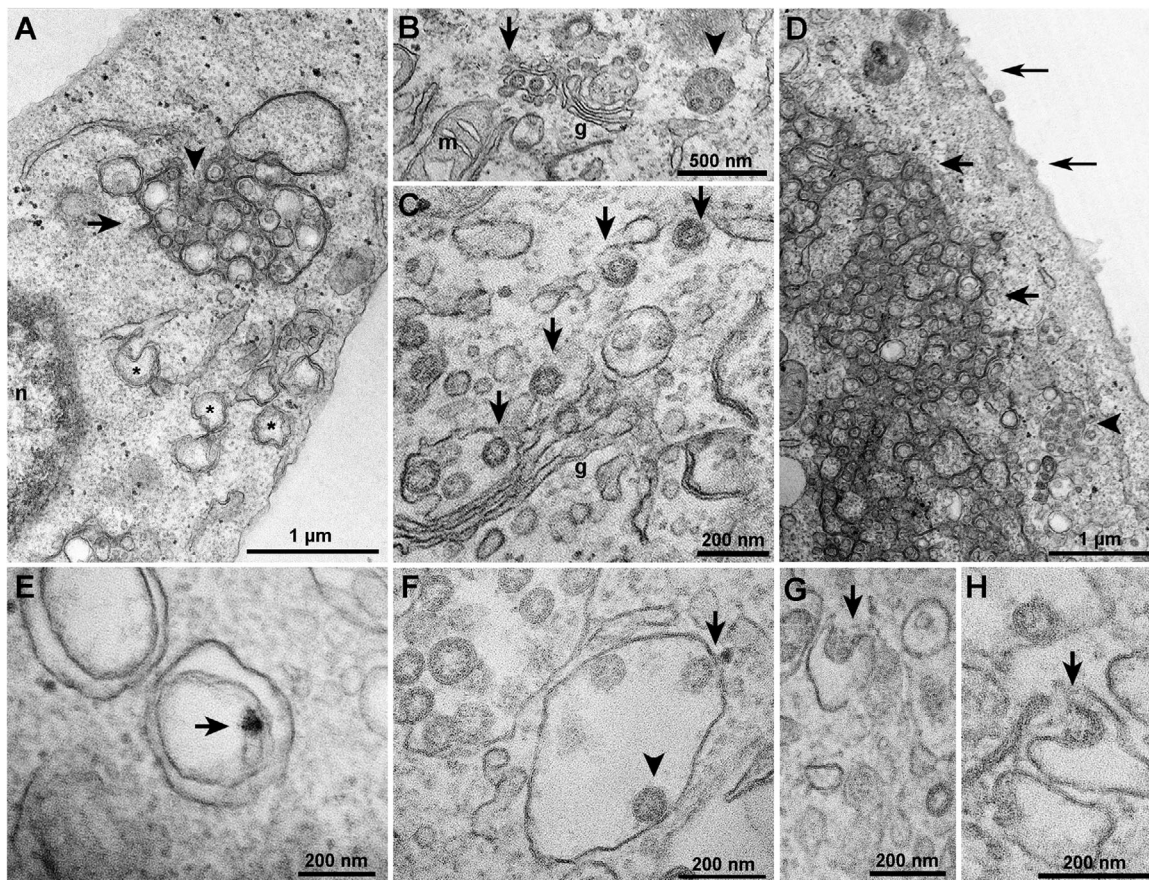

examined (including mock-infected samples), this arrangement was only observed in five cells, all of them from 48 hpi. The size length observed for these arrangements were 1.7, 2, 2.3, 2.4, and 3.4 μm.

At 24 and 48 hpi, the majority of DMVs were ≈340 and 283 nm in size, respectively (Figures 4A and 4B). In the case of LVCVs, the sizes of ≈320 and 800 nm were prevalent at 24 and 48 hpi, respectively (Figures 4C and 4D). The size and frequency of intracellular and extracellular viruses were also analysed. At 24 and 48 hpi, the sizes observed for intracellular viruses were of ≈91 and 79 nm, respectively (Figures 4E and 4F). The size of viruses found at the extracellular domain was predominantly of ≈79 nm (Figures 4G and 4H).

The LVCV was analysed by electron tomography (Figure 5 and Supplemental Material 1). The elected region contained a plethora of smooth vacuoles with intense virus-processing activity (Figure 5A). As a step for SARS-CoV-2 particle assembly, immature viruses were observed budding into large smooth membrane vacuoles. These compartments displayed

Figure 3 | Transmission electron microscopy of late events observed in the SARS-CoV-2 cell cycle (**A**) After budding into the viroplasm membrane arrangements, the nascent virus is still linked to a membrane belt's smooth vacuole membrane (arrow). (**B**) After detachment, the viral particles remain adhered to the inner face of the vacuole (arrows). (**C**) Extensive membrane excerpts were found to participate in the wrapping of more than one SARS-CoV-2 nucleocapsid (arrow), resulting in distinct virus particles. The image in (**D**) shows a smooth vacuole in which virus assembly by budding can be observed (arrowhead), as well as virus adhered to the inner face of the vacuole (arrows) and free luminal virus particles (long arrow). (**E**) A locus in the DMV's interspace displays the association with LCVC (arrow). DMVs are marked with (asterisk). (**F**) At 48 hpi, an organised parallel structure of cisternae-like interspersed with spherical arrangements can be observed next to the Golgi apparatus (g) and multilamellar vesicles (asterisk).
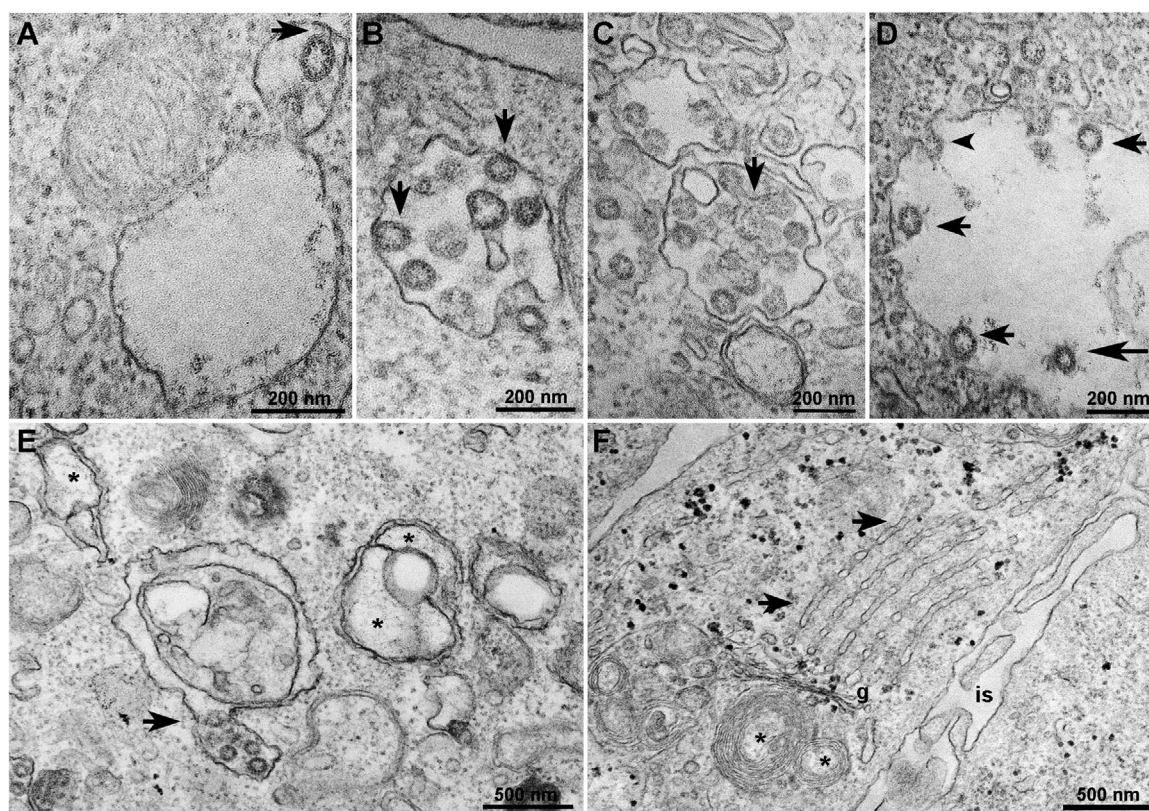
virus particles adhered to their inner layer. The disposition and sizes of viral particles inside the vacuole are shown in Figures 5B and 5C.

To further investigate the interactions of DMVs and vesicular-tubular clusters containing spheroid-like structures, we performed the electron tomography of a selected area in the viroplasm's perinuclear area (Supplemental Material 2) (Figure 6). Along with revealing the connections between the apparently distinct containing-virus compartments (Figures 6A–6D), the tomograms' analysis also revealed the presence of viral particles between the inner and outer nuclear envelope membranes (Figures 6C–6F).

Discussion

There is no current vaccine against SARS-CoV-2 or specific antiviral treatment to COVID-19. In this regard, the investigation of SARS-CoV-2 interaction with the cell can be a promising way to contribute to pharmacological targets. The occurrence of a great variety of membrane alterations in the coronavirus-infected cells was previously pinpointed as an opportunity to explore new potential antivirals (Shahmohamadnejad et al., 2020).

Since the first efforts to study the betacoronavirus morphogenesis using electron microscopy were performed, just after the SARS outbreak of 2002/2003

Figure 4 | Size and frequency of DMVs, LVCVs and virus particles (**A**) At 24 hpi, the majority of vesicles were between 340 and 377 nm in size (*n* = 231). (**B**) At 48 hpi, DMVs of ≈283 nm in size were prevalent (nm = 137). (**C**) The LVCVs observed were predominantly ≈310 nm in size at 24 hpi (*n* = 231) (**D**) and ≈758 nm at 48 hpi (*n* = 33). (**E**) Measuring of intracellular viruses showed the prevailing values of ≈91 nm at 24 hpi (*n* = 210) (**F**) and ≈79 nm at 48 hpi (*n* = 224). (**G**) At 24 hpi, viruses observed at the extracellular medium were ≈82 nm in size (*n* = 75). (**H**) At 48 hpi, the prevalent values were of ≈79 nm (*n* = 44).
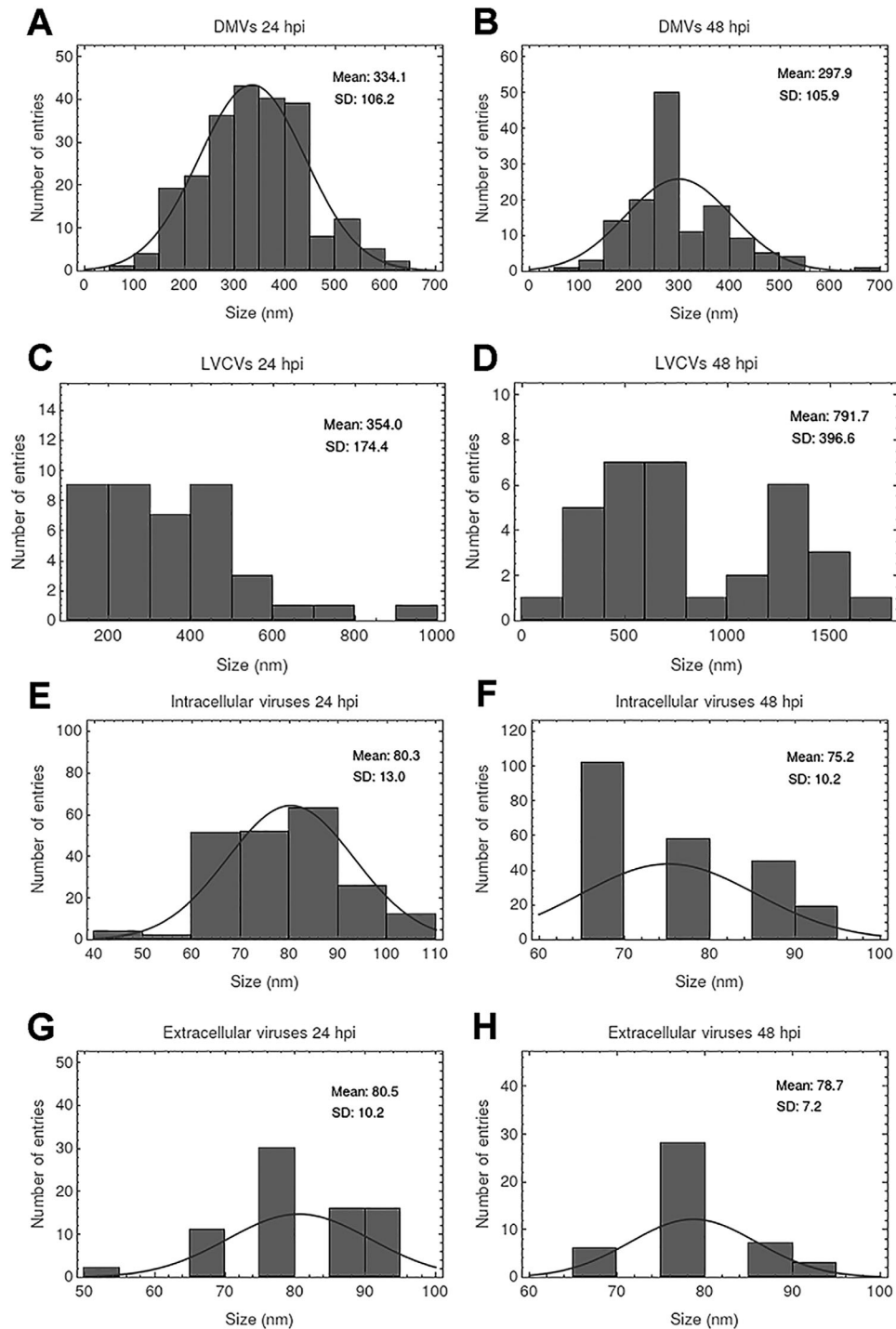
Figure 5 | Electron tomography of the LCVC (A) In the cytoplasm of 48 hpi cells, viruses were observed next to the inner layer of large smooth vacuoles (asterisk). Arrow points to the internalisation into these vacuoles and assembly of these viral particles by budding. The LCVC (arrowhead) is reconstructed in (**B**), where the blue layer corresponds to the vacuolar membrane, and the viruses are coloured in yellow. (**C**) The same LCVC is laterally depicted, showing different sizes (from 45 to 80 nm) for the particles.
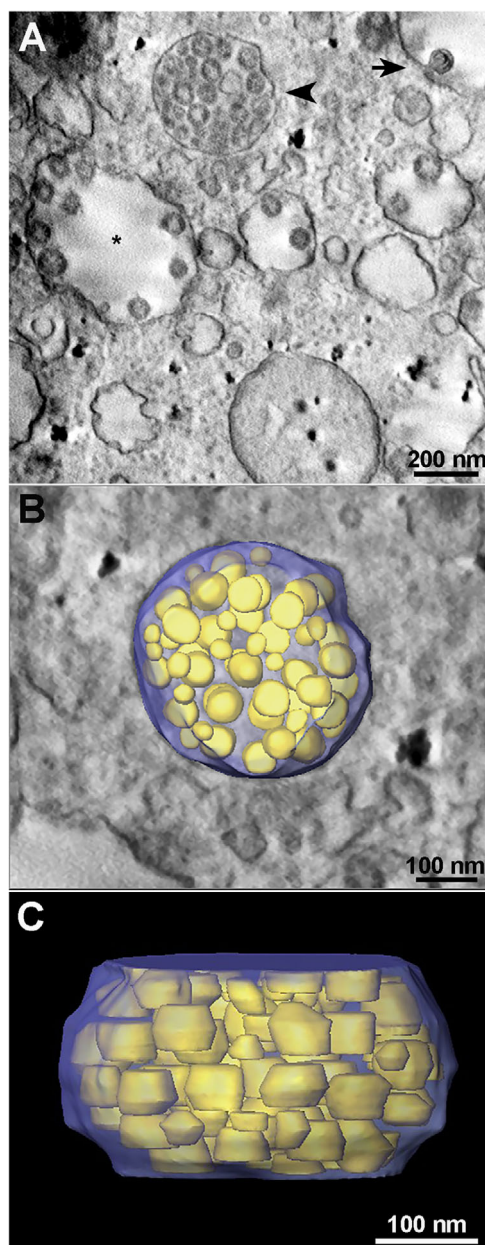
(Ng et al., 2003, 2004), more detailed works approached the plethora of membrane arrangements induced by these coronavirus infections.

Many works on TEM of the infection by different genera of coronavirus identified distinct membrane structures, which were thought to belong specifically to the genera approached in separated studies (Ulasli et al., 2010; Maier et al., 2013; Doyle et al., 2019). The fusion between the "outer membranes" of DMVs is supposed to result in the vesicle packets (Knoops et al., 2008).

The current narrative for SARS-CoV-2 morphogenesis is based on that assumed for SARS-CoV. The viral RNA is synthesised within virus-induced tubular structures that, when transversely sectioned, display the so-called morphology DMVs, followed by the budding of viral particles from the ERGIC membranes. The secretory pathway would be responsible for the egress of virions through exocytosis (Qian et al., 2013; Barreto-Vieira et al., 2020).

In this study, we aimed to explore the main morphological alterations of Vero cells infected by a SARS-CoV-2 isolated from a patient of the state of São Paulo (Brazil). Their crown shape readily identified the viral particles and the electron-dense clusters, corresponding to the nucleocapsid, apposed to the inner side of the envelope membrane (Park et al., 2020; Udugama et al., 2020; Ogando et al., 2020).

Previous works on the coronaviruses morphogenesis suggested that ERGIC-derived DMVs are interconnected through their 'outer membrane' and showed that their interior harbours viral genome (Knoops et al., 2008; Snijder et al., 2020). Subsequent studies on the coronavirus replication complex indicated that RNA might act as a chaperone to the N protein, and the complex is translocated to the CMs and DMVs (Cong et al., 2017). However, the mechanism by which this genetic material crosses the DMV 'internal membrane' was still unsolved until the recent demonstration of a molecular pore connecting the DMV's interior to its exterior (Wolff et al., 2020). The finding of hotspots of electron-dense material in the DMVs inner layer (Figure 2E) and the site of virus budding in smooth vacuoles (Figures 2F–2H) corroborate the translocation of ribonucleoprotein complexes to the sites of virus assembly recently showed by Klein et al. (2020) and previously suggested by SEM (Caldas et al., 2020a). The *en bloc* sample processing used, which included

Figure 6 | Electron tomography of a perinuclear area of SARS-CoV-2 viroplasm

Reconstruction of viroplasm (vp) perinuclear region structures revealed the connections between DMVs and a complex vesicular tubular cluster filled with virus particles. (**A–E**) Separate membrane clusters from smooth vacuoles containing viruses (arrows) have their link exposed. (**C–F**) The tomogram also revealed the presence of viral particles at the nuclear envelope lumen (arrowhead). (**E**) Reconstruction of the perinuclear viroplasm area, with the resolved membranes (blue) and viruses (yellow). (**F**) Represents the area depicted in (**E**). n, nucleus.
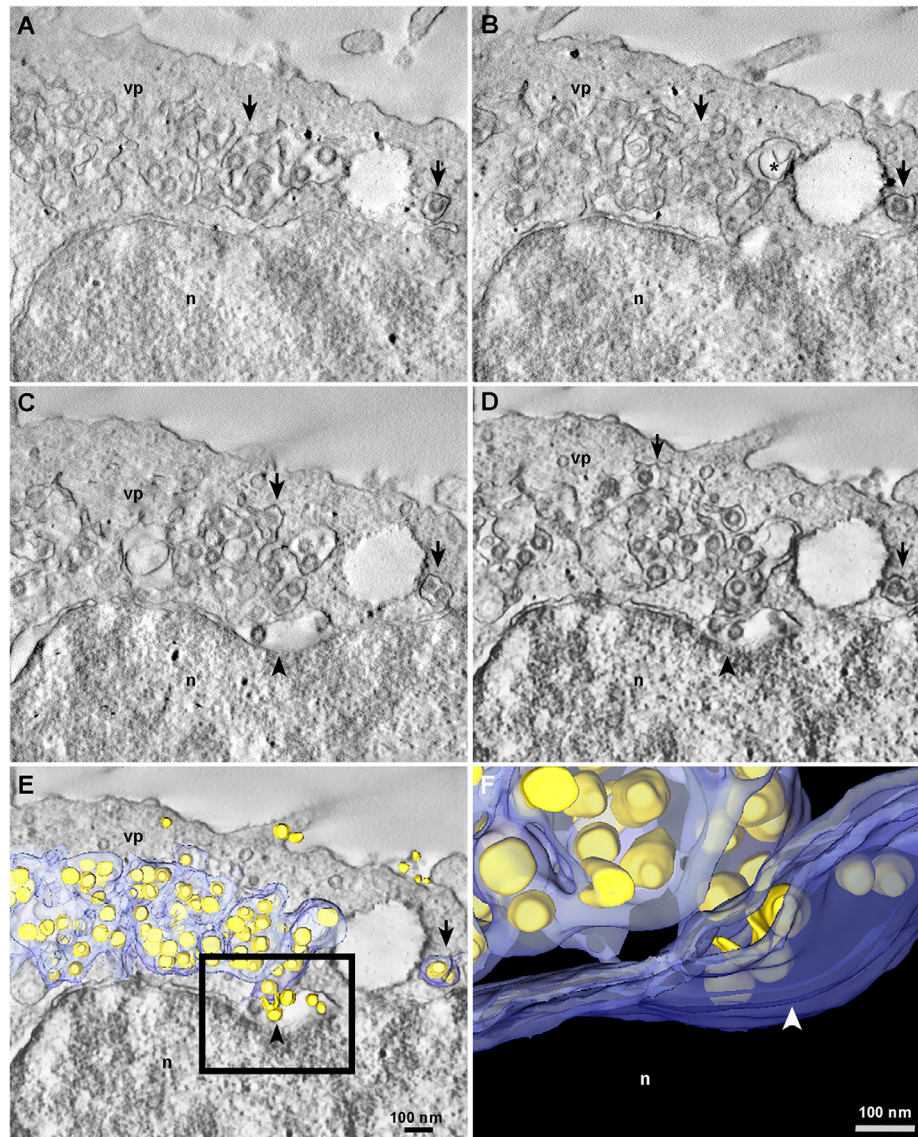
uranyl acetate, previously shown to enhance the visualisation of nucleic acids, highlighted the RNA molecules, reinforcing this interpretation.

Consistent with these findings, SARS-CoV-2 DMVs (Figures 1B and 1E) were found to contain filamentous electron-dense material in a closed inner layer (Figure 1F), whereas the outer layer was contin-

uous with other DMVs (Figure 5 and Supplemental Material 2). In the present study, the average DMVs diameter varied from 120 to 600 nm. However, it is important to note that these values can change according to the sectioned cell area. The presence of zippered ER (Figure 1D) is consistent with the hypothesis of its subsequent wrapping into nascent

DMVs (Figure 2A) (Oudshoorn et al., 2017) and spherules (Maier et al., 2013).

Budding of viruses through the membrane arrangements within the viroplasm results in the nucleocapsid's wrapping by smooth vacuoles membranes. Detaching of virions to the vesicle lumen is preceded by a belt-like membrane link (Figure 3A). After that, viruses become adhered to its inner face (Figure 3B) before they become free in the vacuolar lumen (Figure 3D).

In addition to DMVs, CMs and spherules, we also detected the occurrence of annulate lamellae (Figure 3F) in 10% of the observed sections of 48 hpi SARS-CoV-2-infected cells. Although this structure has been reported to occur in a variety of positive-strand RNA virus infections, for example, the hepatitis A virus (Klinger et al., 2001) and, more recently, Zika virus (Caldas et al., 2020a), it was also present during DNA virus infections (Cardinali et al., 1998).

Unusual membrane profiles were previously reported for coronavirus infections as tubular bodies and cubic membrane structures (Ulasli et al., 2010), but annulate lamellae displays a distinct conformation. Several studies suggest potential roles of annulate lamellae on virus replication, for example, the re-envelopment of the Human Herpesvirus 6 during its maturation step (Torrisi et al., 1999). However, even near the Golgi apparatus and near myelin figures (Figure 3F), no viruses were observed within or around these subcellular arrangements.

The occurrence of the aggregation of SARS-CoV-2 particles in the interspace of DMVs (Figure 3E) suggests that the LCVC arises in this locus. Also, the association of ER and DMVs suggests a secretory path, and consequently, an exosomal route to SARS-CoV-2 egress. The increasing of dilated smooth vacuoles through the viroplasm zone and the occurrence of LVCVs (Figures 2C, 2S and Supplemental Material 1) derived from ERGIC/Golgi expanded compartments that concentrate the SARS-CoV-2 structural proteins (Ulasli et al., 2010; Sicari et al., 2020). In agreement with this suggested route for SARS-CoV-2 morphogenesis, from 24 to 48 hpi we observed a decrease in the size of DMVs and the enlargement of LVCVs (Figures 4A–4D). The differences observed in the sizes of intra and extracellular viruses (Figures 4E–4H) may be due to distinct (prefusion or postfusion) spike conformations (Mendonça et al., 2021).

The SARS-CoV-2 SP-induced LVCVs were further explored in our previous studies using SEM to inspect the infected cell's interior. Consistent with them, the electron tomography carried in the present work allowed the finding of virus particles of different sizes although presenting similar shapes (Figure 5 and Supplemental Material 1), previous corroborating data obtained by SEM and TEM (Caldas et al., 2020b; Zhao et al., 2020). Studies on cryo-electron tomography showed that SARS-CoV-2 acquires its envelope, while budding through the LVCVs, which already display the S protein adhered to their internal face (Figure 3D) (Klein et al., 2020).

Electron tomography of a perinuclear area of a SARS-CoV-2-infected cell revealed viral particles in the nuclear envelope luminal space (Figure 6 and Supplemental Material 2). The replication of most RNA viruses does not depend on nuclear entry as their replication and assembly occurs in the cytoplasm. Still, even for some of these viruses, the nucleocapsid presence within the nucleus is linked to the inhibition of the immune response (Wulan et al., 2015). The mouse hepatitis virus, the infectious bronchitis virus and porcine respiratory and reproductive syndrome virus (PRRSV) are examples of *Nidovirales* members (being the first two representatives of the *Coronaviridae* family) that had their nucleocapsids detected in the cell nucleus during infection, resulting in cell cycle progression inhibition (Wurm et al., 2001; Lee et al., 2006). Although we did not investigate the presence of SARS-CoV-2 nucleocapsid in the nucleus, it was the first time this virus was observed between the inner and the outer nuclear membranes.

Finally, recent studies on SARS-CoV-2 morphogenesis in different cell lines have shown the inner membrane of DMVs within complex tubular structures, or have demonstrated that the DMV outer membrane is contiguous with the ER membrane, or even raised the hypothesis of DMV formation through the ER edge collapse (Mendonça et al., 2020; Cortese et al., 2020). The tubular interconnections that harbour the so-called 'DMV' inner membranes, when transversely sectioned, as in the case of TEM, appear as a configuration that suggests a DMV. Because of this possible artifact, we propose the denomination of tubular compartment-enclosed vesicles (TCEVs) instead of DMVs.

Figure 7 | Schematic drawing of SARS-CoV-2 morphogenesis (**i**) After the viral genome (green) replication within the ER-derived (silver) TCEV, ribonucleoprotein complex (blue) becomes stabilised (**ii**) while migrates to the ERGIC membrane (orange) (**iii**). (**iv**) SARS-CoV-2 acquires its envelope (red) while budding into the ERGIC lumen. ERGIC bilayer's inner face displays the S proteins (purple), which are incorporated into the viral particle upon budding. (**v**) The virus remains adhered to the ERGIC's inner membrane before its full shape fill the lumen of this compartment. This model is based on the present observations and previous studies on this theme, especially those performed by Snijder et al. (2020), Wolff et al. (2020), and Klein et al. (2020).
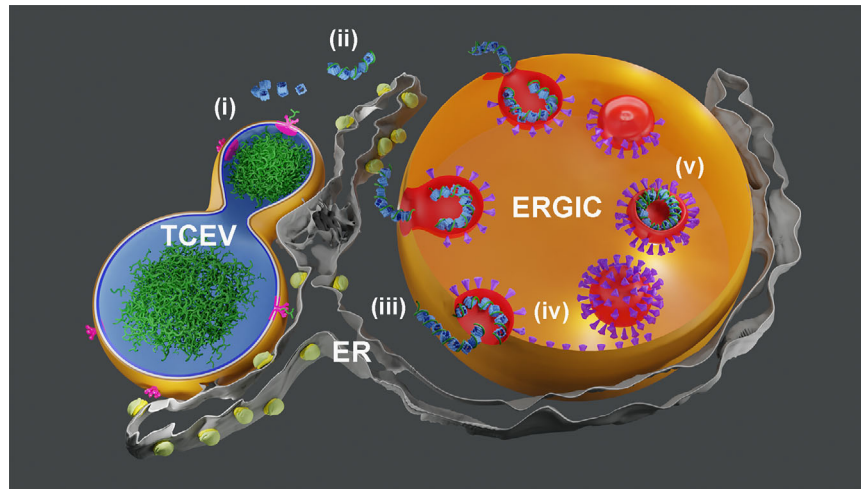
Based on the data presented herein, together with the more recently published works on the mechanisms of interactions between SARS-CoV-2 and host cells, we propose a unified model for some steps of this virus's morphogenesis (Figure 7). In this model, the developing viral genome that resulted from SARS-CoV-2 replication within ER-derived TCEVs (i) is exported through a molecular pore (Snijder et al., 2020; Wolff et al., 2020) to the cytosol, where it associates with clusters of SARS-CoV-2 N protein. This ribonucleoprotein complex packages the newly synthesised viral genome (ii), ensuring its stabilisation during the ERGIC budding zone's translocation. These supercoiled dense structure bud into the ERGIC lumen (iii). The virus acquires its envelope during this process, and at this moment, the inner face of the ERGIC membrane already embodies the S proteins (iv) (Klein et al., 2020). Once the budding is completed, the viruses remain adhered to the inner face of the ERGIC membrane before filling the lumen of this compartment (v).

Conclusion

Since our previous study, we investigated the SARS-CoV-2 SP viroplasm by SEM (Caldas et al., 2020b);

the membrane structures and compartments involved in the replication and morphogenesis of this virus were now studied by TEM herein. Therefore, this work contributes to understanding the interaction mechanisms between SARS-CoV-2 and the host cells, taking into account the general morphological alterations, the recruitment of organelles and cell components in the context of the intense membrane remodelling that takes place during infection. The details of intra-membranar virus budding and the unique features displayed in these positive-strand RNA viruses approached in this study may greatly impact the development of novel antiviral strategies.

Material and methods
Cells and virus

SARS-CoV-2 (HIAE-02: SARS-CoV-2/SP02/ human/2020/B.R.A. (GenBank accession number MT126808.1) was isolated in São Paulo (Brazil) by Edison Luiz Durigon and grown in Vero cells in the Laboratory of Molecular Virology at the Federal University of Rio de Janeiro, Brazil. Vero cells, which were shown to present susceptibility for SARS-CoV-2 infection (Kim et al., 2020; Park et al., 2020), were maintained in DMEM supplemented with 5% foetal

bovine serum (FBS; Gibco) at 37°C and 5% CO_2. All work involving infectious SARS-CoV-2 was performed in a biosafety level (B.S.L.)-3 containment laboratory.

Infection assays

Semi-confluent (70%) cells were grown on sterile tissue culture 25 cm^2 flask infected with multiplicity of infection value of 0.1 of SARS-CoV-2 SP in a free-serum medium. After an absorption period of 1.5 h at 37°C and 5% CO_2, a fresh medium containing 5% FBS was added. Cells were fixed and processed for electron microscopy at 24 and 48 hpi). Three independent assays were performed for each time analysed.

En bloc processing for TEM

For TEM analysis, mock and infected monolayers in 25 cm^2 plastic culture flasks were fixed in 2.5% glutaraldehyde in 0.1 M cacodylate buffer (pH 7.2) and post-fixed for 1 h in 1% OsO_4 0.8% potassium ferrocyanide in the same buffer. Samples were then incubated with 2.5% uranyl acetate in water for 2 h, washed three times in 0.1 M cacodylate buffer (pH 7.2), dehydrated in ethanol and embedded in Polybed resin (Polysciences). Ultrathin sections were stained with 5% uranyl acetate (40 min) and 4% lead citrate (5 min) before observation using Hitachi HT7800 transmission electron microscope equipped with an AMT CMOS 8K camera.

Electron microscopy tomography

For electron tomography, samples processed for TEM were cut in semi-thin (200 nm) serial sections in a Leica EM UC7 ultramicrotome (Leica), collected onto formvar-coated copper slot grids and stained with 5% (w/v) uranyl acetate and lead citrate. Colloidal gold particles (10 nm) (gold colloid; Sigma–Aldrich) were used as fiducial markers during the tilted series' alignment. A single-axis tilt series ($\pm$60° with 1° increment) was collected from the samples using the Xplore3D software in a Tecnai Spirit transmission electron microscope (F.E.I. Company) operating at 120 kV coupled to a '2k×2k' pixel Veleta C.C.D. Camera (Olympus).

Tomographic tilt series were processed using IMOD version 4.9.13 (University of Colorado, USA). Projections were aligned by cross-correlation. The final alignment was performed using 10 nm fiducial gold particles followed by weighted back-projection reconstruction. For visualisation, the reconstructed volumes were processed by a Gaussian and Median filter. Manual segmentation and surface rendering were performed with the Amira software package (Visage Imaging, USA).

Conflict of interest statement

The authors have declared no conflict of interest.

References

Alsaadi, E.A.J. and Jones, I.M. (2019) Membrane binding proteins of coronaviruses. Future Virol. **14**(4), 275–286

Barreto-Vieira, D.F., da Silva, M.A.N., Garcia, C.C., Miranda, M.D., Matos, A.R., Caetano, B., Resende, P.C., Motta, F., Siqueira, M.M. and Barth, O.M. (2020) Morphology and morphogenesis of SARS-CoV-2 in vero-E6 cells. Mem. Inst. Oswaldo Cruz. **116**, e200443. https://doi.org/10.1590/0074-02760200443

Caldas, L.A., Azevedo, R.C., da Silva, J.L. and de Souza, W. (2020a) Microscopy analysis of Zika virus morphogenesis in mammalian cells. Sci. Rep. **10**(1), 8370.

Caldas, L.A., Carneiro, F.A., Higa, L.M., Monteiro, F.L., da Silva, G.P., da Costa, L.J., Durigon, E.L., Tanuri, A. and de Souza, W. (2020b) Ultrastructural analysis of SARS-CoV-2 interactions with the host cell via high resolution scanning electron microscopy. Sci. Rep. **10**(1), 16099

Cardinali, G., Gentile, M., Cirone, M., Zompetta, C., Frati, L., Faggioni, A., Torrisi, M.R. (1998) Viral glycoproteins accumulate in newly formed annulate lamellae following infection of lymphoid cells by human herpesvirus 6. J. Virol. **72**, 9738–9746

Cong, Y., Kriegenburg, F., de Haan, C.A.M. and Reggiori, F. (2017) Coronavirus nucleocapsid proteins assemble constitutively in high molecular oligomers. Sci. Rep. **7**(1), 5740

Cortese, M., Lee, J.Y., Cerikan, B., Neufeldt, C.J., Oorschot, V.M.J., Köhrer, S., Hennies, J., Schieber, N.L., Ronchi, P., Mizzon, G., Romero-Brey, I., Santarella-Mellwig, R., Schorb, M., Boermel, M., Mocaer, K., Beckwith, M.S., Templin, R.M., Gross, V., Pape, C., Tischer, C., Frankish, J., Horvat, N.K., Laketa, V., Stanifer, M., Boulant, S., Ruggieri, A., Chatel-Chaix, L., Schwab, Y. and Bartenschlager, R. (2020) Integrative imaging reveals SARS-CoV-2-induced reshaping of subcellular morphologies. Cell Host Microbe **28**(6), 853–866.e5

Doyle, N., Hawes, P.C., Simpson, J., Adams, L.H. and Maier, H.J. (2019) The porcine deltacoronavirus replication organelle comprises double-membrane vesicles and zippered endoplasmic reticulum with double-membrane spherules. Viruses **11**(11), 1030

Hansen, M.D., Johnsen, I.B., Stiberg, K.A., Sherstova, T., Wakita, T., Richard, G.M., Kandasamy, R.K., Meurs, E.F., Anthonsen, M.W. (2017) Hepatitis C virus triggers Golgi fragmentation and autophagy through the immunity-related GTPase M. Proc. Natl. Acad. Sci. U S A **114**(17), E3462–E3471.

Gillespie, L.K., Hoenen, A., Morgan, G. and Mackenzie, J.M. (2010) The endoplasmic reticulum provides the membrane platform for the biogenesis of the flavivirus replication complex. J. Virol. **84**(20), 10438–10447.

Kim, J.M., Chung, Y.S., Jo, H.J., Lee, N.J., Kim, M.S., Woo, S.H., Park, S., Kim, J.W., Kim, H.M. and Hana, M.G. (2020) Identification of coronavirus isolated from a patient in Korea with COVID-19. Osong Public Health Res. Perspect. **11**(1), 3–7.

Klein S, Cortese, M., Winter, S.L., Wachsmuth-Melm, M., Neufeldt, C.J., Cerikan, B., Stanifer, M.L., Boulant, S., Bartenschlager, R., Chlanda, P. (2020) SARS-CoV-2 structure and replication characterized by in situ cryo-electron tomography. Nat. Commun. **11**(1), 5885

Klinger, M.H., Kämmerer, R., Hornei, B. and Gauss-Müller, V. (2001) Perinuclear accumulation of hepatitis A virus proteins, R.N.A., and particles and ultrastructural alterations in infected cells. Arch. Virol. **146**(12), 2291–2307

Knoops, K., Kikkert, M., Worm, S.H., Zevenhoven-Dobbe, J.C., van der Meer, Y., Koster, A.J., Mommaas, A.M. and Snijder, E.J. (2008) SARS-coronavirus replication is supported by a reticulovesicular network of modified endoplasmic reticulum. PLoS Biol. **6**(9), e226

Lee, C., Hodgins, D., Calvert, J.G., Welch, S.K., Jolie, R., and Yoo, D. (2006). Mutations within the nuclear localization signal of the porcine reproductive and respiratory syndrome virus nucleocapsid protein attenuate virus replication. Virology **346**, 238–250

Lu, R., Zhao, X., Li, J., Niu, P., Yang, B. Wu, H., Wang W., Song H., Huang B., Zhu, N., Bi, Y., Ma, X., Zhan F., Wang, L., Hu, T., Zhou H., Hu, Z., Zhou, W., Zhao, L., Chen, J., Meng, Y., Wang, J., Lin, Y., Yuan J., Xie, Z., Ma, J., Liu, W.J., Wang, D., Xu, W., Holmes, E.C., Gao, G.F., Wu, G., Chen, W., Shi, W. and Tan, W. (2020) Genomic characterization and epidemiology of 2019 novel coronavirus: 456 implications for virus origins and receptor binding. Lancet **20**, 30251–8

Maier, H.J., Hawes, P.C., Cottam, E.M., Mantell, J., Verkade, P., Monaghan, P., Wileman, T. and Britton, P. (2013) Infectious bronchitis virus generates spherules from zippered endoplasmic reticulum membranes. mBio. **4**(5), e00801-13

Mendonça, L., Howe, A., Gilchrist, J.B., Sun, D., Knight, M.L., Zanetti-Domingues, L.C., Bateman, B., Krebs, A.S., Chen, L., Radecke, J., Sheng, Y., Li, V.D., Ni, T., Kounatidis, I., Koronfel, M.A., Szynkiewicz, M., Harkiolaki, M., Martin-Fernandez, M.L., James, W. and Zhang, P. (2020) SARS-CoV-2 assembly and egress pathway revealed by correlative multi-modal multi-scale cryo-imaging. *BioRxiv*. https://doi.org/10.1101/2020.11.05.370239

Miller, S. and Krijnse-Locker, J. (2008) Modification of intracellular membrane structures for virus replication. Nat. Rev. Microbiol. **6**(5), 363–374

Netherton, C.L. and Wileman, T. (2011) Virus factories, double-membrane vesicles, and viroplasm generated in animal cells. Curr. Opin. Virol. **1**(5), 381–387

Ng, M.L., Tan, S.H., See, E.E., Ooi, E.E. and Ling, A.E. (2003) Early events of SARS coronavirus infection in Vero cells. J. Med. Virol. **71**(3), 323–331

Ng, M.L., Lee, J.W.M., Leong, M.L.N., Ling, A-E., Tan, H-C. and Ooi, E.E. (2004) Topographic changes in SARS coronavirus-infected cells at late stages of infection. Emerg. Infect. Dis. **10**(11), 1907–1914

Ogando, N.S., Dalebout, T.J., Zevenhoven-Dobbe, J.C., Limpens, R.W.A.L., van der Meer, Y., Caly, L., Druce, J., de Vries, J.J.C., Kikkert, M., Bárcena, M., Sidorov, I. and Snijder, E.J. (2020) SARS-coronavirus-2 replication in Vero E6 cells: Replication kinetics, rapid adaptation and cytopathology. J. Gen. Virol. **101**(9), 925-940

Oudshoorn, D., Rijs, K., Limpens, R.W.A.L., Groen, K., Koster, A.J., Snijder, E.J., Kikkert, M., and Bárcena, M. (2017). Expression and cleavage of Middle East respiratory syndrome coronavirus nsp3-4 polyprotein induce the formation of double-membrane vesicles that mimic those associated with coronaviral R.N.A. replication. mBio **8**(6), 1–17

Park, W.B., Kwon, N.J., Choi, S.J., Kang, C.K., Choe, P.G., Kim, J.Y., Yun, J., Lee, G.W., Seong, M.W., Kim, N.J., Seo, J.S., and Oh, M.D. (2020) Virus isolation from the first patient with SARS-CoV-2 in Korea. J. Korean Med. Sci. **35**(7), e84

Prentice, E., Jerome, W.G., Yoshimori, T., Mizushima, N. and Denison, M.R. (2004) Coronavirus replication complex formation utilizes components of cellular autophagy. J. Biol. Chem. **279**, 10136–10141

Qian, Z., Travanty, E.A., Oko, L., Edeen, K., Berglund, A., Wang, J., Ito, Y., Holmes, K.V. and Mason, R.J. (2013) Innate immune response of human alveolar type II cells infected with severe acute respiratory syndrome–coronavirus. Am. J. Respir. Cell Mol. Biol. **48**(6), 742–748

Rabaan, A.A., Al-Ahmed, S.H., Haque, S., Sah, R., Tiwari, R., Malik, Y.S., Dhama, K., Yatoo, M.I., Bonilla-Aldana, D.K. and Rodriguez-Morales, A.J. (2020) SARS-CoV-2, SARS-CoV, and MERS-COV: A comparative overview. Index. Med. **28**(2), 174–184

Shahmohamadnejad, S., Nabavi, S.F., Habtemariam, S., Sarkar, K., Sil, P.C., Dowran, R. and Nabavi, S.M. (2020) May we target double-membrane vesicles and oxysterol-binding protein to combat SARS-CoV-2 infection? Cell Biol. Int. **44**(9), 1770–1772

Sicari, D., Chatziioannou, A., Koutsandreas, T., Sitia, R. and Chevet, E. (2020) Role of the early secretory pathway in SARS-CoV-2 infection. J. Cell Biol. **219**(9), e202006005

Snijder, E.J., Limpens, R.W.A.L., Wilde, A.H., de Jong, A.W.M., Zevenhoven-Dobbe, J.C., Maier, H.J., Faas, F.F.G.A., Koster, A.J. and Bárcena, M. (2020) A unifying structural and functional model of the coronavirus replication organelle: Tracking down RNA synthesis. PLoS Biol. **18**(6), e3000715

Spuul, P., Balistreri, G., Kaariainen, L. and Ahola, T. (2010) Phosphatidylinositol 3-kinase-, actin microtubule-dependent transport of semliki forest virus replication complexes from the plasma membrane to modified lysosomes. J. Virol. **84**(15), 7543–7557

Torrisi, M.R., Gentile, M., Cardinali, G., Cirone, M., Zompetta, C., Lotti, L.V., Frati, L. and Faggioni, A. (1999) Intracellular transport and maturation pathway of human herpesvirus 6. Virology **257**, 460–471

Udugama, B., Kadhiresan, P., Kozlowski, H.N., Malekjahani, A., Osborne, M., Li, V.Y.C., Chen, H., Mubareka, S., Gubbay, J.B. and Chan, W.C.W. (2020) Diagnosing COVID-19: The disease and tools for detection. A.C.S. Nano. **14**(4), 3822–3835

Ulasli, M., Verheije, M.H., de Haan, C.A. and Reggiori, F. (2010) Qualitative and quantitative ultrastructural analysis of the membrane rearrangements induced by coronavirus. Cell. Microbiol. **12**(6), 844–861

Walls, A.C., Park, Y.J., Tortorici, M.A., Wall, A., McGuire, A.T. and Veesler, D. (2020) Structure, function, and antigenicity of the SARS-CoV-2 spike glycoprotein. Cell **181**(2), 281–292.e6

Wolff, G., Limpens, R.W.A.L., Zevenhoven-Dobbe, J.C., Laugks, U., Zheng, S., de Jong, A.W.M., Koning, R.I., Agard, D.A., Grünewald, K., Koster, A.J., Snijder, E.J. and Bárcena, M. (2020) A molecular pore spans the double membrane of the coronavirus replication organelle. Science **369**(6509), 1395–1398

World Health Organization. WHO Director- General's opening remarks at the media briefing on COVID-19 - 11 March 2020. (2020) WHO https://www.who.int/dg/speeches/detail/who-director-general-s-openingremarks-at-the-media-briefing-on-covid-19—11-march-2020

Wulan, W.N., Heydet, D., Walker, E.J., Gahan, M.E. and Ghildyal, R. (2015) Nucleocytoplasmic transport of nucleocapsid proteins of enveloped R.N.A. viruses. Front. Microbiol. **6**, 553

Wurm, T., Chen, H., Hodgson, T., Britton, P., Brooks, G. and Hiscox, J.A. (2001) Localization to the nucleolus is a common feature of coronavirus nucleoproteins, and the protein may disrupt host cell division. J. Virol. **75**, 9345–9356

Zaki, A.M., van Boheemen, S., Bestebroer, T.M., Osterhaus, A.D. and Fouchier, R.A. (2012) Isolation of a novel coronavirus from a man with pneumonia in Saudi Arabia. N. Engl. J. Med. **367**(19), 1814–1820

Zhao, J., Zhou, H., Huang, W., Zhou, J., Qiu, M., Deng, Z., Chen, L., Weng, Y., Cai, L., Gu, Y., Zheng, Q., Chen, Q., Hou, X., Wang, L., Shen, L. and Yang, Z. (2020) Cell morphological analysis of SARS-CoV-2 infection by transmission electron microscopy. J. Thorac. Dis. **12**(8), 4368–4373

Zhong, N.S., Zheng, B.J., Li, Y.M., Poon, Xie, Z.H., Chan, K.H., Li, P.H., Tan, S.Y., Chang, Q., Xie, J.P., Liu, X.Q., Xu, J., Li, D.X., Yuen, K.Y., Peiris and Guan, Y. (2003) Epidemiology and cause of severe acute respiratory syndrome (SARS) in Guangdong, People's Republic of China. Lancet **362**(9393), 1353-8

Zhu, N., Zhang, D., Wang, W., Li, X., Yang, B., Song, J., Zhao, X., Huang, B., Shi, W., Lu, R., Niu, P., Zhan, F., Ma, X., Wang, D., Xu, W., Wu, G., Gao, G.F., Phil, D. and Tan, W. (2020) A novel coronavirus from patients with pneumonia in China, 2019. N. Engl. J. Med. **382**, 727–733